Journal of Ship Research, Vol. 46, No. 1, March 2002, pp. 1–15

Journal of
Ship Research

Bow Wave Dynamics

T. A. Waniewski, C. E. Brennen, and **F. Raichlen**

California Institute of Technology, Pasadena, California

Experimental studies of air entrainment by breaking waves are essential for advancing the understanding of these flows and creating valid models. The present study used experimental simulations of a ship bow wave to examine its dynamics and air entrainment processes. The simulated waves were created by a deflecting plate mounted at an angle in a supercritical free-surface flow in a flume. Measurements of the bow wave geometry at two scales and also for a bow wave created by a wedge in a towing tank are presented. Contact line and bow wave profile measurements from the different experiments are compared and demonstrate the similarity of the flume simulations to the towing tank experiments. The bow wave profile data from the towing tank experiments were used to investigate the scaling of the wave with the flow and the dependence on geometric parameters. In addition, surface disturbances observed on the plunging wave are documented herein because of the role they play in air entrainment. The air entrainment itself is explored in Waniewski et al (2001).

1. Introduction

When a displacement-type ship moves through the water, it typically creates a white-water (foamy, aerated, and turbulent) wake. The main sources of air bubbles in these white-water wakes are: bow wave breaking, air entrainment into the ship's turbulent hull boundary layer at the free surface, and ventilation and cavitation of the propeller(s). In recent years, a specific interest in these flows arises from the need for signature estimation from white-water wakes created by U.S. Navy destroyers. These ships travel at over 16 m/s (30 knots), creating wakes which can be several kilometers in length. In addition to being visible to the naked eye, these wakes may be observed by other methods, including microwave radar, synthetic aperture radar, and infrared radiometry (Peltzer 1984).

Despite the complexity of these multi-phase flows, numerical models have been developed and computations performed. Carrica et al (1998) demonstrated that the bubbles introduced at the bow of the ship have significant effects on the wake; however, this study and others lack an accurate model for the bow wave air entrainment process and use arbitrary bubble sources unrelated to the flow parameters. Increasing the realism of these calculations depends on including accurate models for the bow wave air entrainment process (perhaps similar to Baldy's (1993) model for bubbles created by wind waves), and experimental work is the key to developing them.

The present study used a simulated bow wave produced using a stationary deflecting plate in a supercritical free surface flow in a recirculating free surface water channel. This stationary, simulated bow wave allowed for detailed examination of the breaking process. Additional towing tank experiments using similar models and flow conditions confirmed that this was a valid simulation. This paper focuses on how the bow wave changed with the flow and geometric parameters. An earlier paper describes the measurements of the air entrainment process (Waniewski et al 2001).

2. Experimental equipment

Stationary model experiments were conducted in a 40 m long recirculating and tilting flume with a slope of 1 vertical to 50 horizontal; it is referred to herein as the large flume. It was 109 cm wide with 1.3 cm thick tempered glass sidewalls and a stainless steel bottom plane to within ±2.5 mm. The large flume was filled with city tap water at about 23°C. The flow rate, Q, was measured to within ± 0.0014 m^3/s using a 41 cm Venturi meter in the recirculating system; the maximum discharge was approximately 0.394 m^3/s. To create the supercritical flow needed for this type of experiment, a two-dimensional spillway section was installed at the upstream end of the flume, downstream of a 8.1 m long reservoir. The mean velocity of this flow was $U = Q/A$

Manuscript received at SNAME headquarters August 5, 1999; revised manuscript received August 14, 2001.

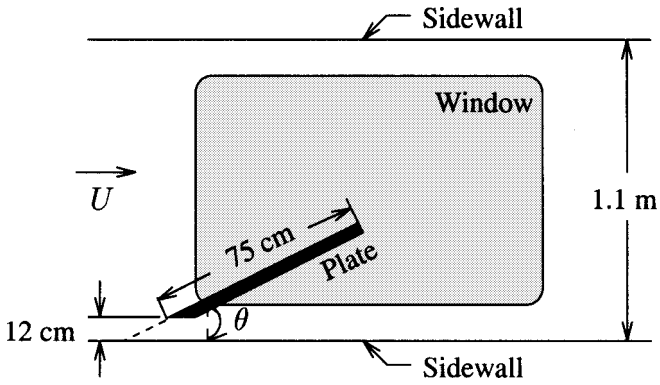

Fig. 1 Plan view of test section in 40 m flume

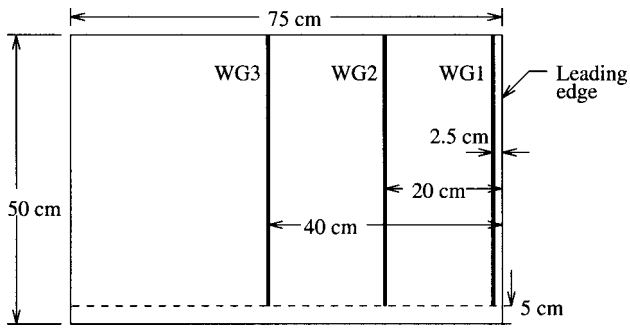

Fig. 2 View of deflecting plate with wave gages marked

where $A = 1.09 \cdot d$ m^2 and d was the depth measured upstream of the deflecting plate using a point gage. The test section was located approximately 24 m, or over 200 depths, downstream of the spillway.

A 75 cm long and 50 cm high Lucite plate was mounted in the test section at an angle θ to the oncoming flow to simulate a wedge-shaped hull with half angle θ (Fig. 1). Its leading edge was displaced 12 cm from the flume sidewall. The dihedral angle, ϕ, the angle between the plate surface and the undisturbed free surface, also could be changed. A steady breaking wave similar to that observed at the bow of a ship is created as the flow rides up on the plate.

Stationary model experiments also were conducted in a much smaller recirculating glass bottom tilting flume, 265 cm long and 45.9 cm wide which will be termed the small flume. It was filled with tap water at about 23°C. The flow was adjusted using both a flow control valve downstream of the pump and a flap nozzle located at the entrance to the flume. This generated supercritical flows approximately 1 cm deep. A mercury/water manometer connected to an orifice meter was used to determine the flow rate, Q, to within ± 100 cm^3/s; the maximum flow rate was about 0.01 m^3/s. The velocity of the flow was $U = Q/A$ where $A = 0.459 \cdot d$ m^2. The 12 cm high and 42 cm long Lucite deflector plate was 35 cm downstream of the flume inlet, and its leading edge was located a few centimeters from the flume side wall.

The towing tank experiments were conducted in a 126 m long, 7.5 m wide, and 3.7 m deep tank at Hydronautics Research, Inc. in Fulton, Maryland. This was filled with fresh water at about 16°C. Two wedge models with bow half angles of 13 deg and 26 deg were used, each with 1.3 cm thick Lucite sidewalls and 0.64 cm thick aluminum bottoms. The maximum velocity of the towing carriage was approximately 5.2 m/s, and the draft could be changed from about 5 cm to 25 cm.

In the flume experiments, the elevation of the surface of the bow wave was measured using an electronic point gage. The tip of this gage was a sharpened stainless steel rod 1.64 mm in diameter, and the water surface elevation was defined when the tip of the rod was in contact with the water surface 50% of the time. In the small flume, the point gage was positioned manually to within ± 1 mm in the streamwise direction, ± 0.5 mm in the cross stream direction, and ± 1 mm in the vertical direction. In the large flume, the point gage was positioned to within ± 0.03 mm in the streamwise direction and ± 0.6 mm in the cross stream direction using stepper motors. A feedback system activated a motor which adjusted the vertical position of the gage to the pre-set contact time percentage (Waniewski 1999). The expected error in these elevation measurements is also less than ± 1 mm.

In the large flume, three flush-mounted wave gages were used to measure the oscillation of the free surface height on the deflecting plate. Each wave gage consisted of a pair of electrodes spaced 0.64 cm apart. Figure 2 shows the deflecting plate with the location of the gages marked. Although there was some run up and splashing on the wave gages, the oscillations of the free surface could be measured. Free surface oscillations in the flume reservoir upstream of the spillway also were measured using a resistance type wave gage. Further details are given in Waniewski (1999).

Nomenclature

d = upstream depth or model draft (m)
$\mathbf{F}$ = Froude number based on upstream conditions, $\mathbf{F} = U/\sqrt{gd}$
$\mathbf{F}_1$ = Froude number based on upstream water depth, $\mathbf{F}_1 = U/\sqrt{gd}$
$\mathbf{F}_2$ = Froude number based on model draft, $\mathbf{F}_2 = U/\sqrt{gd}$
g = gravitational acceleration (m/s^2)
l_{max} = location of maximum elevation in r-direction (cm)
Q = flume volumetric flow rate (m^3/s)
r = horizontal coordinate along deflecting plate
r' = nondimensional coordinate along deflecting plate, $r' = r/\mathbf{F}d$
$\mathbf{R}$ = Reynolds number, $\mathbf{R} = U\,d\rho/\mu$
U = upstream velocity (m/s)
U_i = jet velocity at impact (m/s)
$\mathbf{W}$ = Weber number, $\mathbf{W} = \rho U^2 d/\sigma$
x = streamwise coordinate
y = cross stream coordinate
z = vertical coordinate
Z = free surface height
Z^* = nondimensional free surface elevation, $Z^* = Z/(\mathbf{F}^{1.5} \cdot d \cdot 2\theta/180)$
Z_{max} = maximum free surface elevation (cm)
β = angle of impingement (deg)
μ = dynamic viscosity (kg/ms)
ν = kinematic viscosity (m^2/s)
ϕ = dihedral angle (deg)
ρ = density (kg/m^3)
θ = wedge half-angle (deg)

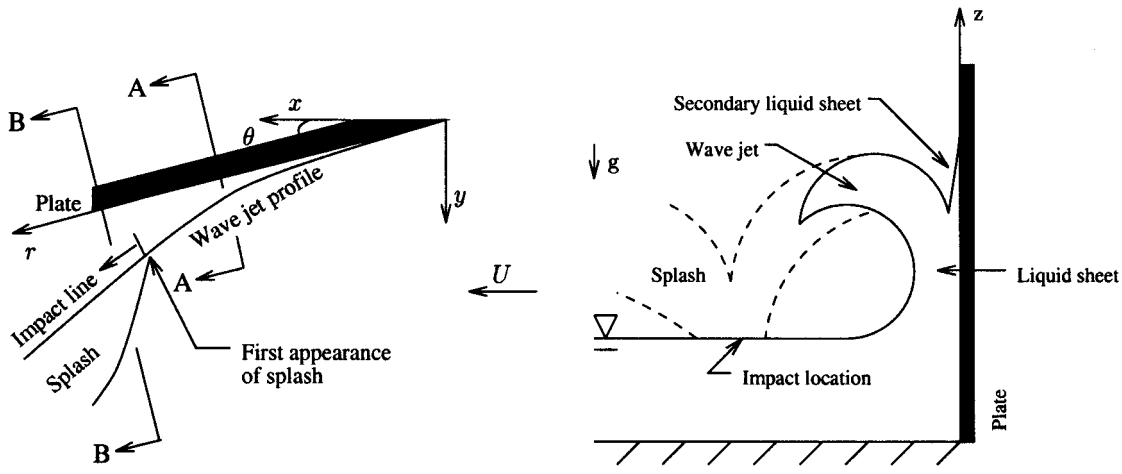

(a) Planview of the bow wave created by the deflecting plate.

(b) Cross-sectional views at A (—) and B (- -) of the planview. The horizontal coordinate along the deflecting plate, r, is perpendicular to the plane of the paper.

Fig. 3 Schematic of main features of bow wave. Undisturbed free surface is $z = 0$ cm and leading edge of deflecting plate is at $(x, y) = (0, 0)$

3. Experimental observations

In the flume experiments, the bow wave generated by the deflecting plate transitioned through three distinct regimes depending on the Froude number, $\mathbf{F}_1$. For subcritical flow conditions, the plate created a disturbance extending 5 cm to 10 cm upstream of the leading edge. At critical flow conditions, a wave similar to an oblique hydraulic jump was observed ahead of the plate. Then, for supercritical flow conditions, a wave similar to a bow wave was formed. Figure 3 presents an exaggerated schematic of the bow wave with the key features labeled. In all cases, the free surface was unsteady and turbulent on and behind the wave front. These flow regimes also were observed in the towing tank experiments where a Froude number based on draft rather than depth characterized the flow. Miyata & Inui (1984) observed similar waves in their towing tank experiments.

It is important to emphasize the key role which the flow at the leading edge plays in determining the geometry and height of the bow wave. Noblesse et al (1991) demonstrated this analytically, and concluded that the flow direction must be vertical at the free surface/leading edge intersection. Just how critical this local flow is to subsequent development of the bow wave is demonstrated by the photographs in Fig. 4. In Fig. 4(a), the leading edge of the deflecting plate is against the flume wall and "turns" the flow creating a wave similar to an oblique hydraulic jump. On the other hand, in Fig. 4(b) the deflecting plate is at the same angle to the flow as in Fig. 4(a), but it is displaced from the flume wall by 2.5 cm. In contrast to Fig. 4(a) (where the vertical velocity at the intersection of the wall and the deflecting plate must be zero), the vertical velocity at the bow in Fig. 4(b) creates a liquid sheet which has an elevation above the free surface at the leading edge! This initial elevation has been reported by other researchers as well (see, for example, the photographs of the recent towed ship model experiments by Dong et al (1997)). The liquid sheet then continues to ride up on the plate before it separates and forms the bow wave. Note that the height of the run-up is much greater than in Fig. 4(a), presumably because the leading edge is outside the wall boundary layer. In Fig. 4(b), as the flow moves away

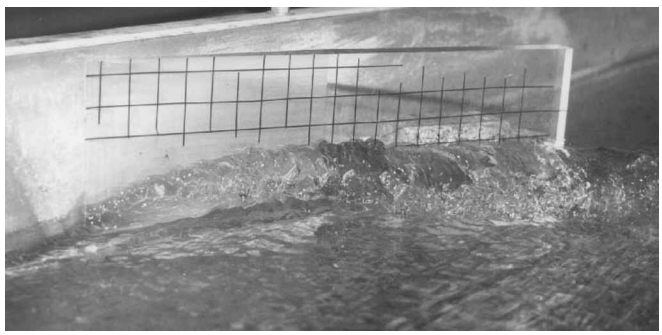

(a) Leading edge against the flume wall.

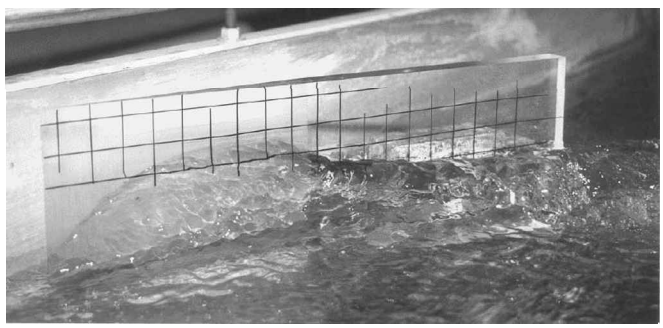

(b) Leading edge displaced 2.5 cm away from the flume wall.

Fig. 4 Photographs of bow waves in 2.6 m flume; flow is from left to right. The grid on deflecting plate is 2 cm by 2 cm, and $\theta = 25$ deg, $\phi = 0$ deg, $U = 1.58$ m/s, $d = 1.21$ cm, and $\mathbf{F}_1 = 4.59$

from the plate, it continues in the upward direction so that the maximum height of the bow wave is located a few centimeters away from the deflecting plate. A thin secondary liquid sheet is observed on the plate surface in the experiments as shown schematically in Fig. 3(*b*). The water in this secondary liquid sheet seemed to result from the unsteadiness of the contact line on the plate.

Returning now to the general description depicted in Fig. 3, once the wave has reached its maximum height, gravity causes it to plunge back towards the free surface as shown in cross section B-B in Fig. 3(*b*). Moreover, inspection of the breaking wave jet reveals almost equally spaced striations along the surface oriented perpendicular to the wave crest; these will be discussed further in section 9 and in Waniewski et al (2001). The edge of the breaking wave is irregular and decomposes into individual jets or strings of droplets as it impacts the free surface along a line we call the impact line (Fig. 3(*a*)). The impact causes a splash region shown schematically in Fig. 3. Although the majority of the splash is formed by the wave jet "bouncing" off the undisturbed free surface, flow visualization tests showed that some of the freestream flow also enters the splash.

The waves generated in the towing tank experiments, where the ratio of the wedge draft to the tank depth varied from 0.014 to 0.068, were similar to the waves generated in the flume experiments. Quantitative similarities will be discussed in section 5. Also, even though the waves created in towing tank experiments had a glassier appearance and a steadier contact line (since the water in the towing tank was quiescent), roughnesses or striations were still observed on the bow waves in these experiments. Photographs of the waves from the flume experiments and the towing tank experiments are included as Fig. 5.

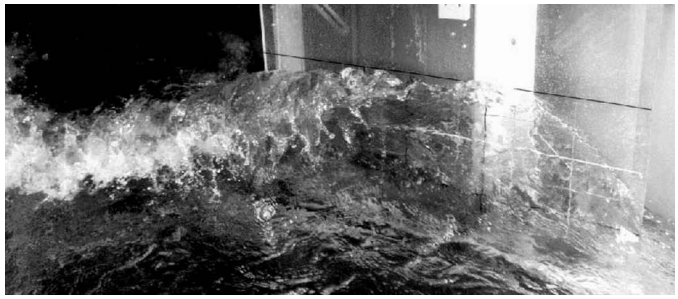

(a) Large flume experiment.

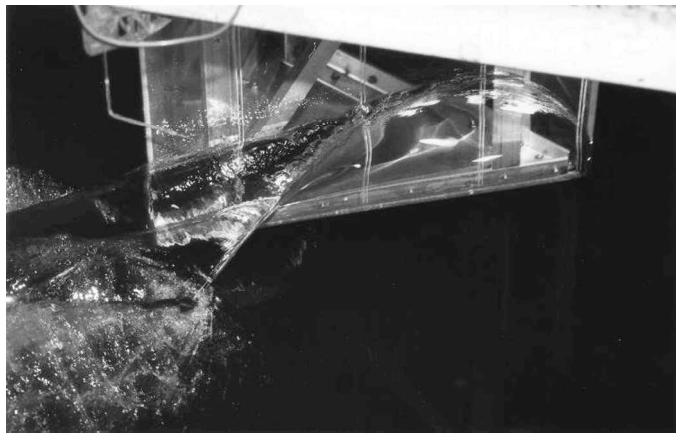

(b) Towing tank experiment.

Fig. 5 Photographs of bow waves for conditions with similar velocity and draft in 40 m flume (flow is from right to left) and in towing tank (wedge is moving to right)

4. Contact line and bow wave profile results

The contact line of the bow wave on the plate surface was measured in both the large and small flume experiments using the free surface probe (section 2) and these data are shown in Fig. 6. Table 1 lists the corresponding flow conditions.

The bow wave profile, the profile of the maximum free surface height of the wave, was measured in the towing tank and the large flume experiments. The profiles were determined using digitized images of the bow wave; each point along the profile could be specified to the nearest pixel, or ±4 mm. The camera was oriented perpendicular to the model sidewall, and its field of view encompassed the entire wall. Initial measurements confirmed the repeatability of these measurements (Waniewski 1999). Figure 7 presents a summary of the data from the towing tank experiments, and Table 2 lists the flow conditions corresponding to each symbol. Here $r = 0$ corresponds to the leading edge, and $z = 0$ corresponds to the location of the undisturbed free surface. For some of the higher velocity runs in the towing tank experiments, the crest of the bow wave was not in the field of view of the camera. In these runs, the model generated a spray sheet which was quite different from the bow wave shown in Fig. 5(*b*); the sheet would often break up into droplets before the maximum elevation was achieved.

These data from the flume and the towing tank experiments will be presented and compared in nondimensional form later in sections 5 and 8.

5. Comparison of flume and towing tank measurements

We first address the issue of whether the flume experiments generated waves similar to those created by a ship's bow in the towing tank experiments. To do so, we compare the maximum elevations of the wave profiles above the undisturbed free surface, $Z_{\max}$, in the large flume and towing tank experiments. For reasons discussed later in section 8, a nondimensional $Z_{\max}$ denoted by $Z^*_{\max}$ is defined as

$$Z^*_{\max} = \frac{Z_{\max}}{\mathbf{F}^{1.5} \cdot d \cdot \frac{2\theta}{180}} \tag{1}$$

The resulting values of $Z^*_{\max}$ are presented as a function of Froude number in Fig. 8. Ogilvie's (1972) results from towing tank experiments also have been added in addition to the maximum height of the contact line in the present small flume experiments. This figure suggests that the flume and towing tank experiments yield similar results and that the water depth and model draft to depth ratio does not have a significant effect on the bow wave profile.

6. Theoretical analyses of contact line

Two different theoretical analyses of the contact line were explored in Waniewski (1999). The first approach was an

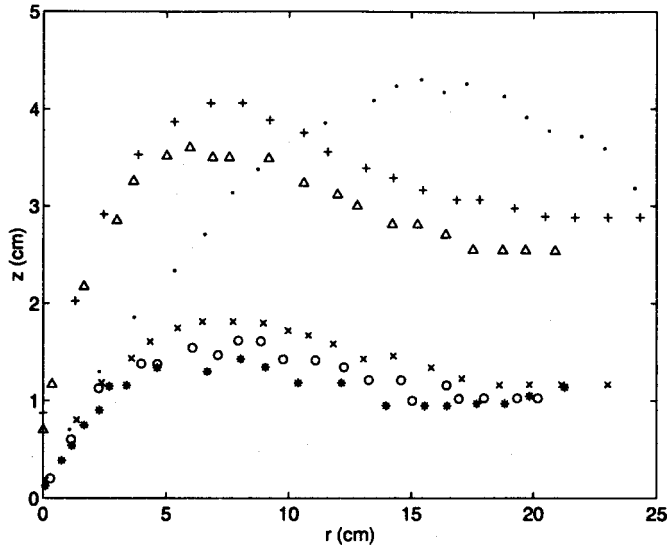

(a) Small flume experiments; (·) for run 1s, (×) for run 2s, (○) for run 3s, (∗) for run 4s, (+) for run 5s, and (△) for run 6s.

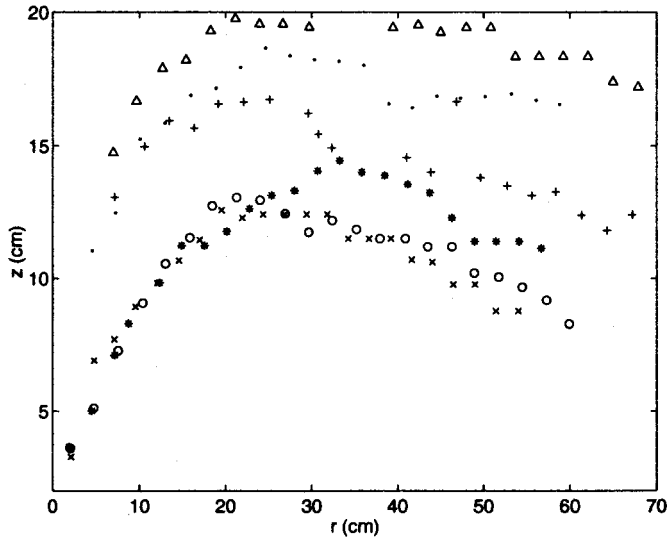

(b) Large flume experiments; (×) for run 1l, (○) for run 2l, (∗) for run 3l, (·) for run 4l, (+) for run 5l, and (△) for run 6l.

Fig. 6 Summary of contact line results from flume experiments. The error in r was 0.9% for small flume experiments and ?% for large flume experiments. In both experiments, elevation was measured to ±1 mm

extension of Ogilvie's (1972) slender body theory to the case of a wedge-shaped bow in a flow of finite depth which is equal to the draft. This approach essentially linearizes the problem in the y-direction, and cannot capture the sudden changes in free surface height which occur near the bow particularly at the leading edge. The solution underestimates our experimental wave heights by an order of magnitude, and does not predict the discontinuity in the free surface elevation observed at the leading edge (see Fig. 4). It was also compared to the contact line elevation solution for a

Table 1 Conditions explored in flume experiments

Run	Experiment	θ (°)	U (m/s)	d (cm)	$\mathbf{F}_1$
1s	Small flume	13.2	1.97	0.95	6.46
2s	Small flume	13.2	1.11	1.35	3.06
3s	Small flume	13.2	1.07	1.35	2.93
4s	Small flume	13.2	0.94	1.35	2.57
5s	Small flume	26.3	1.11	1.35	3.06
6s	Small flume	26.3	1.07	1.35	2.93
1l	Large flume	13.4	2.44	6.66	3.01
2l	Large flume	13.4	2.43	7.55	2.81
3l	Large flume	13.4	2.46	9.21	2.59
4l	Large flume	26.6	2.61	6.45	3.29
5l	Large flume	26.6	2.40	7.62	2.77
6l	Large flume	26.6	2.46	9.32	2.57

vertical wave maker moving horizontally with a step velocity in a fluid of finite depth presented by Joo et al (1990). Their contact line solution is closer both in shape and in magnitude to the experimental results. Using the results they present in their Fig. 5, for a flow with $U = 2.50$ m/s, $d = 7.54$ cm, and $\mathbf{F} = 2.91$ a maximum elevation of 25.9 cm is predicted at a distance $r = 21.7$ cm downstream of the leading edge. This compares well with the data presented in Fig. 4.6 in Waniewski (1999). For this reason, it appears that the analyses explored by Waniewski has other deficiencies in addition to those arising from the linearization, for example, the neglect of surface tension which Joo et al include. Note that Joo et al's solution is not valid for very small times which corresponds to regions very close to the bow. They emphasize that the nonlinear effects must be considered here. Other researchers, including Noblesse (1983), used slender body theory and reported similar difficulties predicting bow wave shapes especially at the leading edge. We conclude that slender body theory is inappropriate for flows around a wedge shape bow; according to Fontaine (1997) this is because the theoretical fluid acceleration is infinite at the leading edge. The second approach pursued by Waniewski (1999) considered perturbations of planar potential flow around a finite hull body but is valid only for Froude numbers less than unity.

Other researchers have used a "parabolic" approximation of the equations called the "2D + t" (two dimensions plus time) theory. This approach reduces the three-dimensional nonlinear stationary problem to a set of two-dimensional transient problems; a literature review may be found in Fontaine & Tulin (1998). In fact, the first analytical approach explored by Waniewski (described above) corresponds to the 2D + t linear solution taking into account the finite depth of the tank. A physical interpretation of the 2D + t approximation is given in Fontaine & Tulin (1998) as follows. First, flow cross sections perpendicular to the velocity of the ship and stationary with respect to the fluid are considered. In these cross sections, the flow appears to be generated by a two-dimensional wave maker which corresponds to the ship hull. In other words, the time variation of the hull cross-sectional area (in the aforementioned flow cross section) generates nonlinear diverging waves. Results for the flow around a wedge shaped bow using this approximation may be found in Fontaine & Cointe (1997) and also Fontaine & Faltinsen (1997), and the numerical results appear promising. The free surface at the leading edge is predicted; however, the elevation is less than

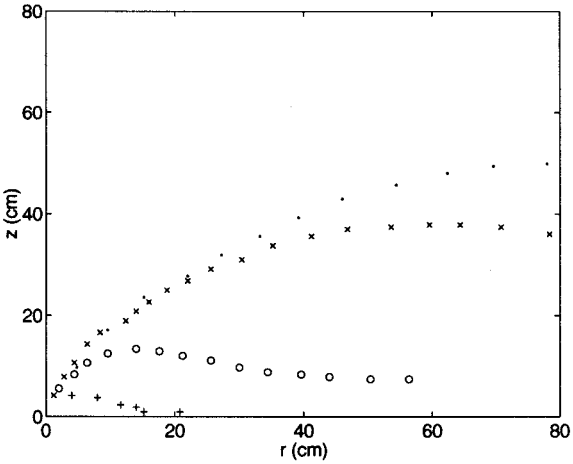

(a) $d = 4.95$ cm; (+) for $U = 1.00$ m/s and $\mathbf{F}_2 = 1.43$, (∘) for $U = 1.99$ m/s and $\mathbf{F}_2 = 2.86$, (×) for $U = 4.01$ m/s and $\mathbf{F}_2 = 5.76$, and (·) for $U = 5.41$ m/s and $\mathbf{F}_2 = 7.77$.

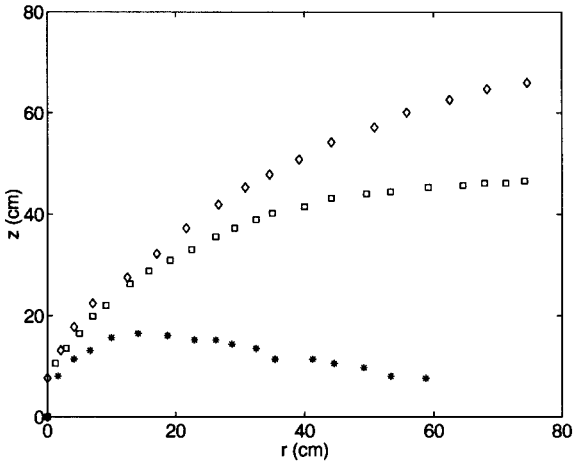

(b) $d = 9.91$ cm; (∗) for $U = 1.98$ m/s and $\mathbf{F}_2 = 2.01$, (□) for $U = 4.00$ m/s and $\mathbf{F}_2 = 4.06$, and (◇) for $U = 5.41$ m/s and $\mathbf{F}_2 = 5.49$.

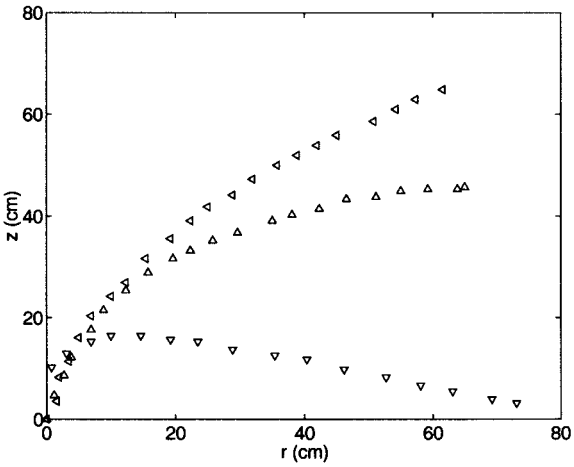

(c) $d = 14.86$ cm; (▽) for $U = 2.01$ m/s and $\mathbf{F}_2 = 1.66$, (△) for $U = 4.00$ m/s and $\mathbf{F}_2 = 3.31$, and (◁) for $U = 5.33$ m/s and $\mathbf{F}_2 = 4.41$.

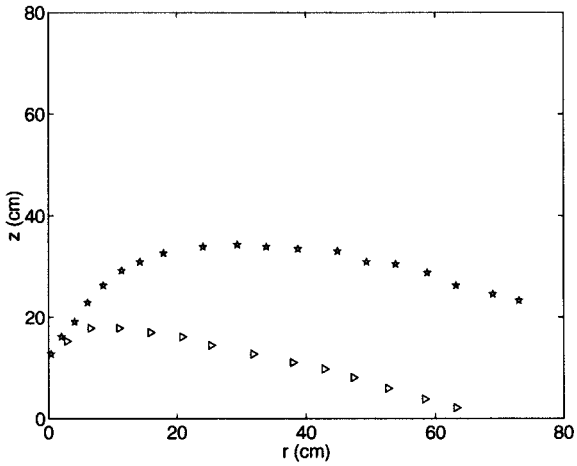

(d) $d = 25.14$ cm; (▷) for $U = 2.00$ m/s and $\mathbf{F}_2 = 1.27$, and (⋆) for $U = 2.94$ m/s and $\mathbf{F}_2 = 1.87$.

Fig. 7 Summary of bow wave profile results from towing tank experiments, $\theta = 26$ deg. Each point along profile was specified to nearest pixel, or ±4 mm

the experimental measurement by approximately a factor of two. Perhaps this is because their expression is valid for high Froude numbers ($\mathbf{F} \gg 1$) whereas their experiments were performed for Froude numbers ranging from 0.56 to 1.5.

7. Plunging jet shape

In the flume experiments, the free surface elevation was measured for different flow cross sections to study the developing shape of the plunging wave jet. Describing this feature of the bow wave is important not only for understanding the three-dimensional structure of the waves, but also for understanding the air entrainment process. As described in Waniewski et al (2001), many researchers have identified the jet size, jet velocity, and impingement angle as key parameters for modeling air entrainment by plunging jets. In these experiments, the jet size and impingement angle were measured directly, and the jet velocity was calculated (Waniewski 1999).

In the large flume experiments, cross sections were measured along sections perpendicular to the direction of the upstream flow using the free surface probe (section 2) at three different streamwise locations for each flow condition. Figure 9 presents a typical result which shows both the exterior and interior surfaces of the jet. The data describing the interior surface is limited by the large amount of splash in this region of the flow which caused incorrect gage readings; however, there were adequate data to define the jet thickness to be about 3 cm. It should also be noted that, for these measurements, the jet did not break up into the strings of droplets described later in section 10.

Table 2 Bow wave profile experimental conditions, $\theta = 26$ deg

Symbol	Experiment	U (m/s)	d (cm)	**F**
●	Large flume	2.46	7.54	2.86
■	Large flume	2.39	6.68	2.95
▲	Large flume	2.22	4.86	3.22
+	Towing tank	1.00	4.95	1.43
○	Towing tank	1.99	4.95	2.86
x	Towing tank	4.01	4.95	5.76
·	Towing tank	5.41	4.95	7.77
✡	Towing tank	2.50	7.54	2.91
*	Towing tank	1.98	9.91	2.01
□	Towing tank	4.00	9.91	4.06
◇	Towing tank	5.41	9.91	5.49
▽	Towing tank	2.01	14.86	1.66
△	Towing tank	4.00	14.86	3.31
◁	Towing tank	5.33	14.86	4.41
▷	Towing tank	2.00	25.14	1.27
★	Towing tank	2.94	25.14	1.87

In the towing tank experiments, flow frontal aspects were measured from digitized images of the bow wave. The camera was secured to the carriage and oriented with the axis of the lens parallel to one side of the wedge so that its field of view encompassed the entire wave cross section. A typical image is shown in Fig. 10. Figure 11 shows the bow wave frontal aspects for five different run conditions having nearly the same velocity. Note that the y^*-coordinate is perpendicular to the side of the wedge rather than the oncoming stream as in the large flume results. The leading edge of the wedge is located approximately at $y^* = 0$, and the undisturbed free surface at the leading edge of the wedge

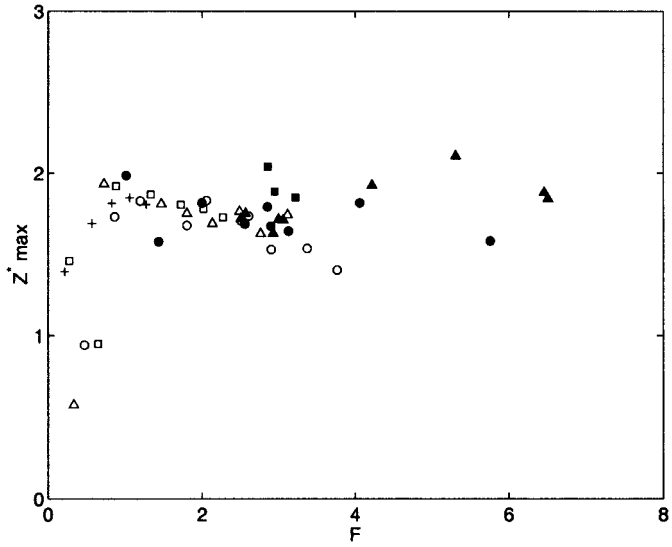

Fig. 8 Nondimensional maximum wave profile elevation, Z^*_{max}, as a function of Froude number, **F**, for flume and towing tank experiments. Small flume experiments (▲) have $\theta = 13.4$ deg, large flume experiments (■) have $\theta = 26.8$ deg, and towing tank experiments (●) have $\theta = 26$ deg. For Ogilvie's towing tank experiments, $\theta = 15$ deg and (○) for $d = 10.2$ cm, (△) for $d = 20.4$ cm, (□) for $d = 30.5$ cm, and (+) for $d = 40.6$ cm

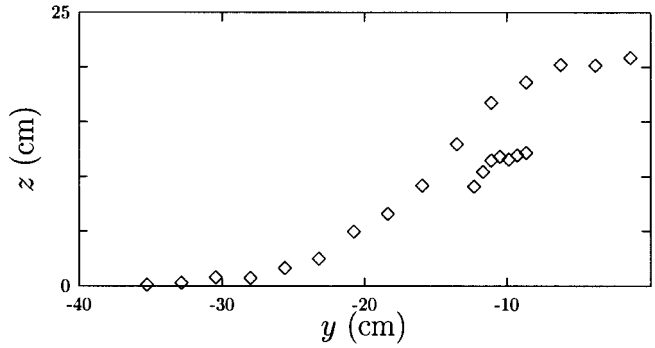

(a) Jet cross-section at $x = 69.1$ cm.

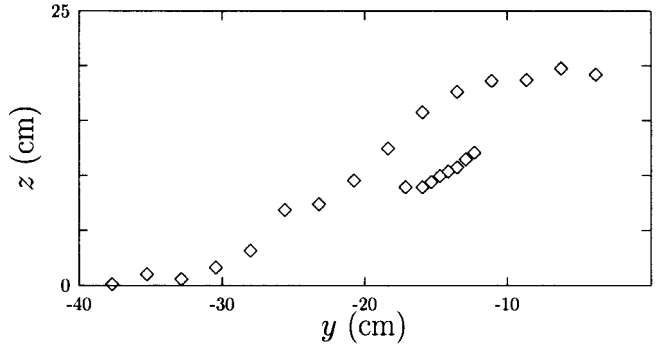

(b) Jet cross-section at $x = 64.0$ cm.

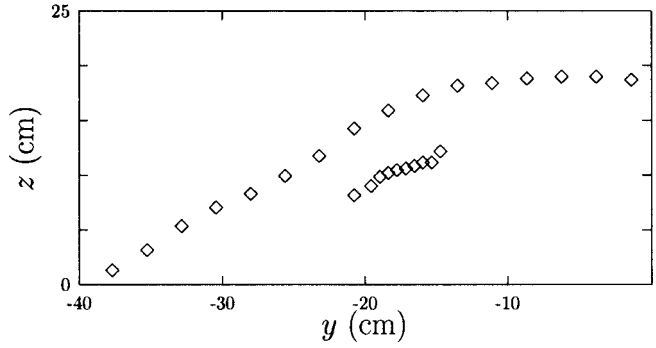

(c) Jet cross-section at $x = 58.9$ cm.

Fig. 9 Cross sections of plunging wave jet in large flume experiments ($\theta = 25.4$ deg) for different distances downstream of the deflecting plate leading edge; $U = 2.39$ m/s, $d = 9.47$ cm, and $\mathbf{F}_1 = 2.48$

is located at $z = 0$. These results demonstrate the repeatability of this measurement technique, and show a jet which is about 2 cm to 3 cm thick with an angle of impingement, β, relative to the undisturbed free surface of about 58 deg. Note the many similarities of the jets formed in the flume and towing tank experiments as shown in Figs. 9, 10, and 11.

Since the plunging wave jet is in free-fall just before impact, it is possible to calculate the horizontal water particle velocity at the crest of the plunging breaker, U_b, using the angle of impingement, β, and the free-fall height, h_f, determined from Fig. 11 and the

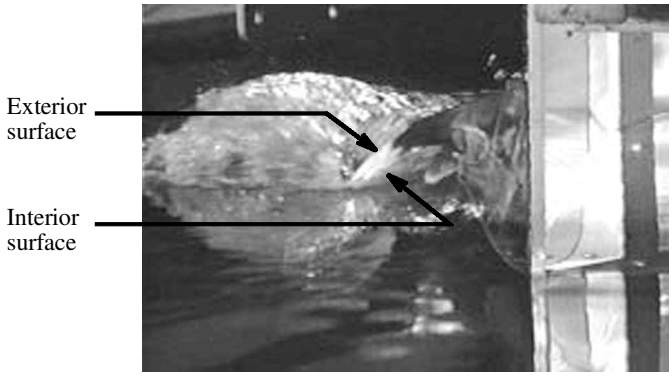

Fig. 10 A frame from video of plunging jet in towing tank experiments for $\theta = 26$ deg, $U = 2.50$ m/s, and $d = 7.54$ cm. Camera is looking at bow of model parallel to starboard side

equation

$$\tan(\beta) = \frac{\sqrt{2gh_f}}{U_b} \tag{2}$$

The jet velocity at impact, U_i, also can be calculated from

$$U_i = \sqrt{U_b^2 + 2gh_f} \tag{3}$$

For $\beta = 58$ deg and $h_f = 20$ cm, equations (2) and (3) give $U_b = 1.2$ m/s and $U_i = 2.3$ m/s, reasonable values since the towing speed was 2.5 m/s.

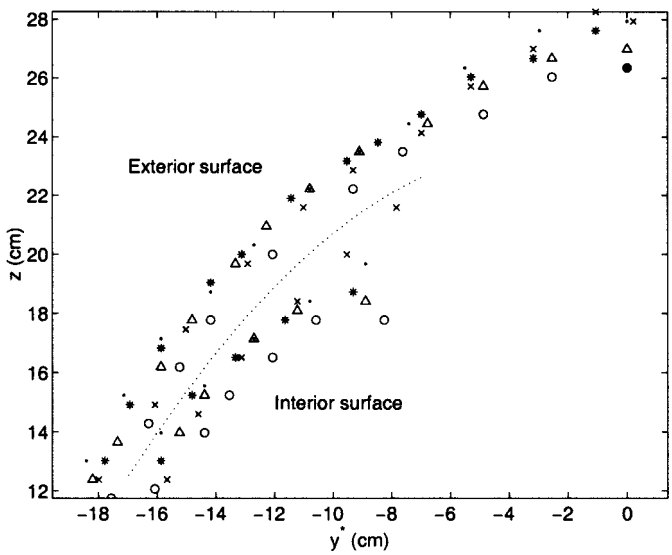

Fig. 11 Frontal aspects of plunging wave jet in towing tank experiments for $d = 7.54$ cm and $\theta = 26$ deg. Symbols indicate velocity: (×) for $U = 2.48$ m/s, (∘) for $U = 2.50$ m/s, (∗) for $U = 2.50$ m/s, (·) for $U = 2.50$ m/s, and (△) for $U = 2.50$ m/s. The dotted line separates exterior jet surface data from interior jet surface data

8. Scaling analysis and considerations

Understanding the manner in which these waves scale is necessary to extend laboratory experiments to flows for ship hulls of various shapes operating at different speeds and drafts. In this section, we develop a relation for the maximum free surface elevation, $Z_{\max}$ and its distance from the leading edge of the deflecting plate, $l_{\max}$. The functional relationship which describes the wave shape is

$$z = f(U, g, d, r, \mu, \rho, \theta, \phi) \tag{4}$$

which also can be expressed by equations

$$z = f_1(U, g, d, \mu, \rho, \theta, \phi) \text{ for a given } r \tag{5}$$

and

$$r = f_2(U, g, d, \mu, \rho, \theta, \phi) \text{ for a given } z \tag{6}$$

By the Buckingham Pi theorem, equations (5) and (6) are equivalent to

$$\frac{z}{d} = f_3(\mathbf{F}, \mathbf{R}, \theta, \phi) \text{ for a given } \frac{r}{d} \tag{7}$$

and

$$\frac{r}{d} = f_4(\mathbf{F}, \mathbf{R}, \theta, \phi) \text{ for a given } \frac{z}{d} \tag{8}$$

where $\mathbf{R} = (U\, d\rho)/\mu$ is the Reynolds number based on upstream flow conditions. Thus, the normalized maximum free surface elevation, $Z_{\max}/d$, and the normalized distance from the leading edge to the maximum, $l_{\max}/d$, can be expressed independently as functions of the flow parameters $\mathbf{F}$ and $\mathbf{R}$ and the geometric parameters θ and ϕ as

$$\frac{Z_{\max}}{d} = f_5(\mathbf{F}, \mathbf{R}, \theta, \phi) \tag{9}$$

and

$$\frac{l_{\max}}{d} = f_6(\mathbf{F}, \mathbf{R}, \theta, \phi) \tag{10}$$

We continue this section by using the experimental data to seek functions f_5 and f_6.

We examine first the bow wave profile data from the towing tank experiments since these encompassed a wider range of flow conditions (velocities and drafts) than the flume experiments. The maximum elevation of the bow wave profile, $Z_{\max}$, is plotted against velocity in Fig. 12(a). Note that these are the same data that were presented in Fig. 8. Figure 12(a) demonstrates quite convincingly that $Z_{\max} \propto U^{1.5}$; the linear curve fit was $Z_{\max} = 5.64U^{1.49}$ using the method of least squares. Consequently, $Z_{\max}/U^{1.5}$ was plotted against draft in Fig. 12(b). This suggests that $Z_{\max}/U^{1.5} \propto d^{0.25}$; the linear curve fit was $Z_{\max}/U^{1.5} = 3.67d^{0.189}$. We conclude that

$$\frac{Z_{\max}}{d} \propto U^{1.5} d^{-0.75}$$

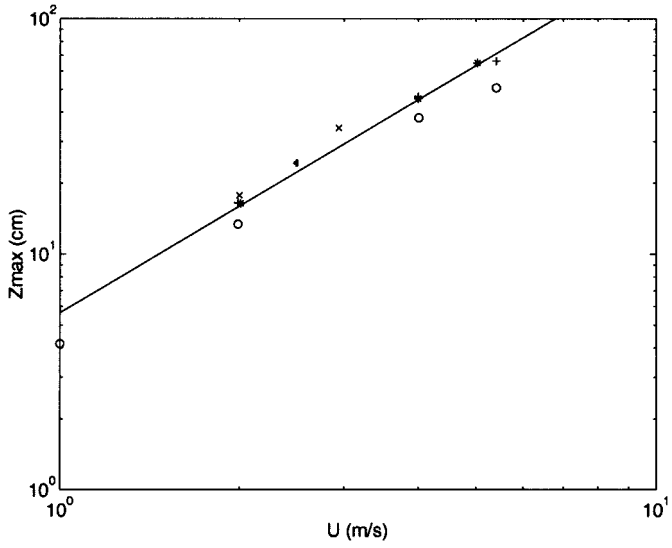

(a) Z_{max} as a function of U; (∘) for $d = 4.95$ cm, (·) for $d = 7.54$ cm, (+) for $d = 9.91$ cm, (*) for $d = 14.86$ cm, and (×) for $d = 25.14$ cm. The equation of the line shown is $Z_{max} = 5.64U^{1.50}$.

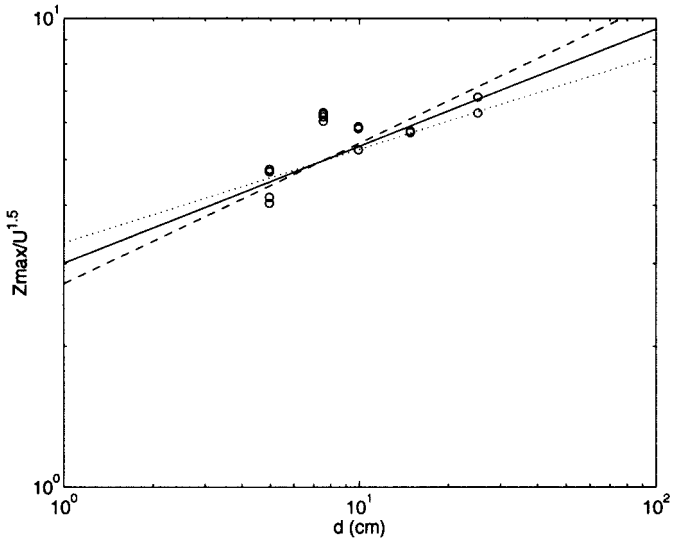

(b) $Z_{max}/U^{1.5}$ as a function of d; the lines are (···) for $Z_{max}/U^{1.5} = 3.32d^{0.20}$, (—) for $Z_{max}/U^{1.5} = 3.00d^{0.25}$, and (--) for $Z_{max}/U^{1.5} = 2.72d^{0.30}$.

Fig. 12 Scaling of maximum wave elevations from towing tank experiments with velocity and draft shown on logarithmic scales

therefore, equation (9) becomes

$$\frac{Z_{\max}}{d} = \mathbf{F}^{1.5} \cdot f_7(\theta, \phi) \tag{11}$$

and this normalized maximum appears to be independent of the Reynolds number within the parameter range investigated. This relationship also is apparent in Fig. 8 for the flume experiments and Ogilvie's towing tank experiments.

A similar procedure was applied to the $l_{\max}/d$ data to investigate the scaling in the r-direction. The result (Waniewski 1999) was that

$$\frac{l_{\max}}{d} \propto U^2 d^{-1.5}$$

thus, equation (10) becomes

$$\frac{l_{\max}}{d} = \mathbf{F}^{7/3}\mathbf{R}^{-1/3} \cdot f_8(\theta, \phi) \tag{12}$$

The results from this scaling analysis do not agree with the scaling derived by Ogilvie (1972), nor with the scaling derived by Waniewski (1999) using an alternative analytical approach. For a given θ and ϕ, Ogilvie derived the nondimensionalization $Z' = Z/\mathbf{F}d$ and Waniewski (1999) derived the nondimensionalization $Z' = Z/d$. Intuitively, it seems that distances in the z-direction should scale with some combination of the velocity head, $U^2/2g$ (or $\mathbf{F}^2 d$), and the draft, d, though it is unclear which length would be more important. Perhaps both Ogilvie's and Waniewski's analyses include assumptions which mask the true scaling seen in the experiments. We are particularly suspicious of the treatment of the flow near the leading edge for the reasons described in section 3.

In the r-direction, Ogilvie derived the nondimensionalization $r' = r/\mathbf{F}d$. The scaling relation in equation (12) includes a Reynolds number and is quite different. The Reynolds number provides an appropriate scaling with velocity and draft (for the towing tank experiments), but it is not possible to verify this using the present database. We speculate, however, that viscous effects could influence flow at the leading edge, and therefore, the location of the maximum wave elevation, $l_{\max}$. For example, if the kinematic viscosity, ν, increased, the Reynolds number would decrease, and according to the scaling relation $l_{\max}$ would move downstream from the leading edge. This seems correct because an increase in ν would also cause an increase in the shear stress on the plate. Then, the flow would lose energy in overcoming this shear stress and take longer to achieve its maximum.

The scaling described in the preceding paragraphs was then applied to the data from all of the bow wave profile experiments, and the results for $\theta = 26^\circ$ are presented in Fig. 13. Theoretically, all of the data should collapse onto a single profile. Figure 13 demonstrates good agreement of the wave profiles near the leading edge; however, the profiles deviate somewhat further downstream, particularly for $d = 4.95$ cm and 7.54 cm. Nevertheless, the experimental data suggest a scaling with flow parameters which is not explained by the existing theoretical analyses but makes some intuitive physical sense.

The preceding discussion was confined to a particular wedge angle, θ, and dihedral angle, ϕ; however, we now seek functions f_7 and f_8 from equations (11) and (12). We begin by examining the effects of the model bow half angle, θ, on the contact lines of the waves using the flume results. Recall that Ogilvie suggested the free-surface height scaled linearly with bow half angle as in equation (1). Using this idea along with the flow parameter scaling discussed above, the free surface height was nondimensionalized by

$$Z^* = \frac{Z}{\mathbf{F}^{1.5} \cdot d \cdot \frac{2\theta}{180}}$$

and the distance in the r-direction was nondimensionalized by $l_{\max}$. The resulting dimensionless profiles are presented in Fig. 14.

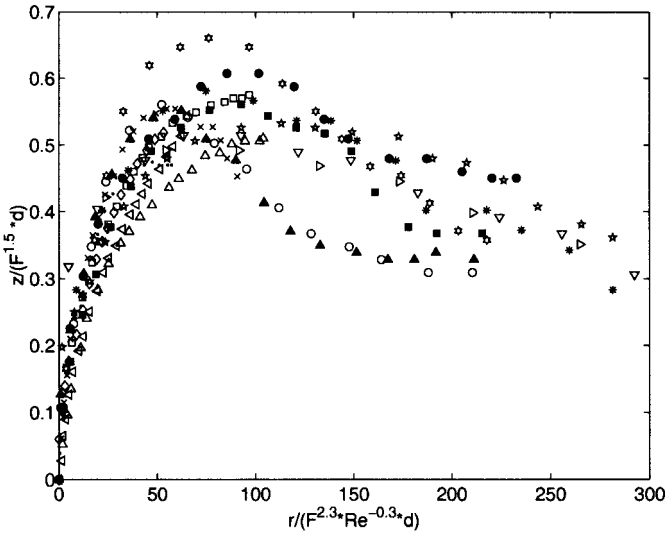

Fig. 13 Nondimensional bow wave profile data for $\theta = 26$ deg shown as $z)(\mathbf{F}^{1.5}d)$ plotted against $r)(\mathbf{F}^{2.3} \cdot \mathbf{R}^{-0.3} \cdot d)$. Open symbols represent towing tank experiments and filled symbols represent large flume experiments. Flow conditions for all of different symbols are listed in Table 2

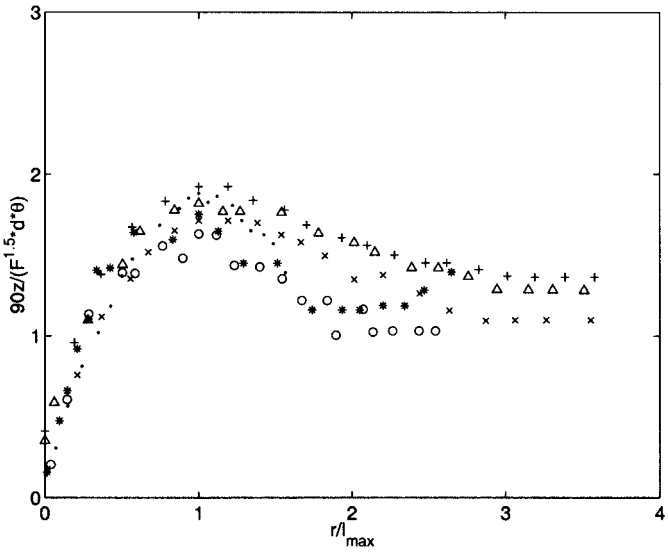

(a) Small flume experiments; (×) for run 1s where $\theta = 13.2°$, (○) for run 2s where $\theta = 13.2°$, (∗) for run 3s where $\theta = 13.2°$, (·) for run 4s where $\theta = 13.2°$, (+) for run 5s where $\theta = 26.3°$, and (△) for run 6s where $\theta = 26.3°$.

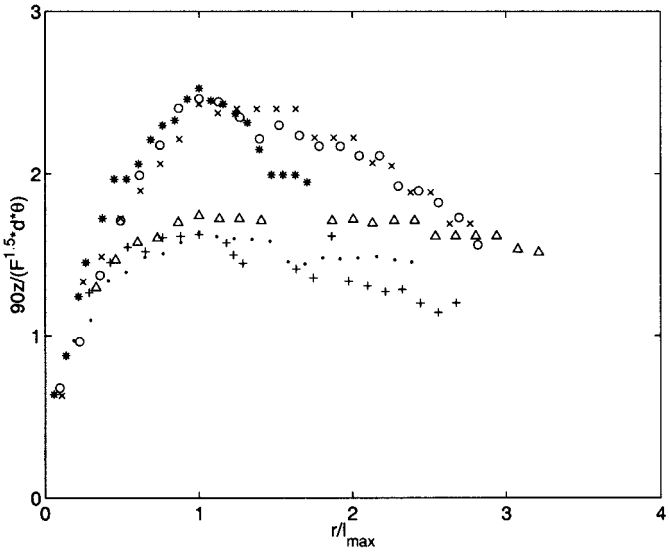

(b) Large flume experiments; (×) for run 1l where $\theta = 13.4°$, (○) for run 2l where $\theta = 13.4°$, (∗) for run 3l where $\theta = 13.4°$, (·) for run 4l where $\theta = 26.6°$, (+) for run 5l where $\theta = 26.6°$, and (△) for run 6l where $\theta = 26.6°$.

Fig. 14 Nondimensional contact lines from flume experiments for different bow half angles

For the small flume experiments, the scaling appears to work reasonably well. For the large flume experiments, the scaling seemed to overcompensate for the larger bow half-angle. This might be due simply to experimental error in measuring the contact line which was very unsteady in those experiments. However, it is also possible that the bow wave does not scale linearly with angle θ as suggested by Ogilvie and that a more complicated nonlinear relationship exists.

We now examine the effect of the model dihedral angle, ϕ, on the waves using results from the small flume experiments. The dihedral angle, the angle between the face of the deflecting plate and the vertical plane, was varied from 0 deg to 15 deg. The results are presented in Fig. 15: Fig. 15(a) is for $\mathbf{F}_1 \approx 3$, Fig. 15(b) for $\mathbf{F}_1 \approx 4$, and Fig. 15(c) for $\mathbf{F}_1 \approx 5$. The data show that the contact line is only weakly dependent on the dihedral angle; however, the elevation of the contact line does appear to increase as the dihedral angle increases, and one hypothesis could be that $Z \propto 1/\cos(\phi)$.

In summary, the experimental data indicate that the free surface elevations scale approximately linearly with the bow half-angle, θ, and are only weakly dependent on the dihedral angle, ϕ.

9. Surface disturbances

Surface disturbances were observed on the plunging face of the bow wave in both the flume and towing tank experiments, and were recorded using various photographic techniques. The surface disturbances appeared as striations or "finger-like" structures on the plunging face of the wave in all of the experiments. The "fingers," the crests of the disturbances, were aligned perpendicular to the wave jet profile and the spacing between successive "fingers" seemed regular as shown schematically in Fig. 16. The disturbances were barely visible near the leading edge of the plate and grew in amplitude as they convected downstream along the crest of the bow wave. They also grew in length, stretching as the liquid sheet fell away from the plate to form the plunging face of the wave.

The upstream flow conditions significantly affected the appearance of the surface disturbances. In the large flume experiments, the surface of the wave was visibly rough due to the upstream flow conditions and this obscured the surface disturbances. Figure 5(a) demonstrates this point. The upstream conditions could be more carefully controlled in the small flume

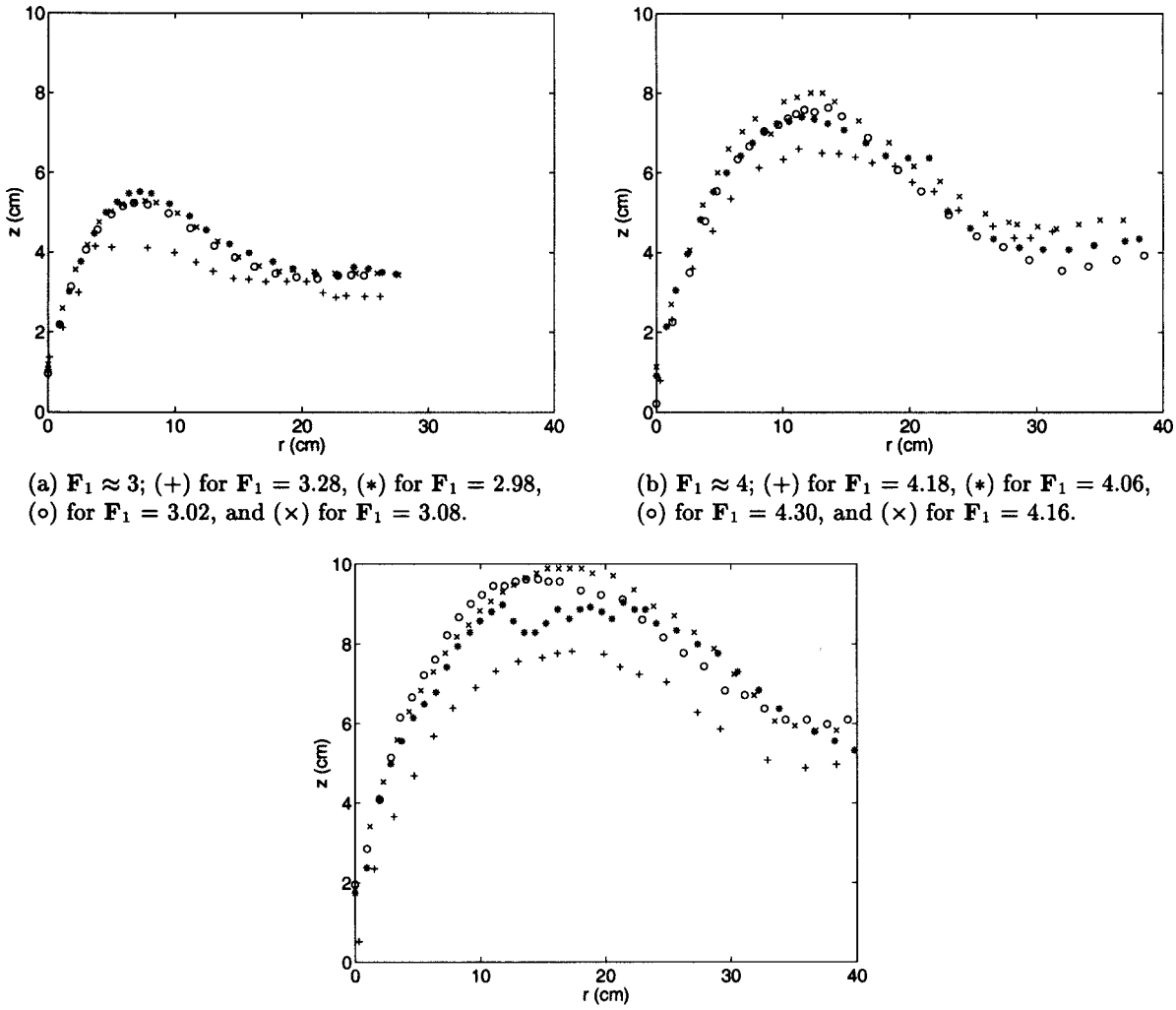

(a) $\mathbf{F_1} \approx 3$; (+) for $\mathbf{F_1} = 3.28$, (∗) for $\mathbf{F_1} = 2.98$, (∘) for $\mathbf{F_1} = 3.02$, and (×) for $\mathbf{F_1} = 3.08$.

(b) $\mathbf{F_1} \approx 4$; (+) for $\mathbf{F_1} = 4.18$, (∗) for $\mathbf{F_1} = 4.06$, (∘) for $\mathbf{F_1} = 4.30$, and (×) for $\mathbf{F_1} = 4.16$.

(c) $\mathbf{F_1} \approx 5$; (+) for $\mathbf{F_1} = 5.37$, (∗) for $\mathbf{F_1} = 5.22$, (∘) $\mathbf{F_1} = 4.70$, and (×) $\mathbf{F_1} = 5.40$.

Fig. 15 Effect of dihedral angle on the contact line for small flume experiments; (+) for $\phi = 0$ deg, (∗) for $\phi = 5$ deg, (∘) for $\phi = 10$ deg, and (×) for $\phi = 15$ deg

experiments and the disturbances on the wave can be seen in Fig. 4. The waves in the towing tank experiments had the smoothest surface; therefore, it was easier to distinguish the surface disturbances. Frames of a video from these experiments are included in Fig. 17.

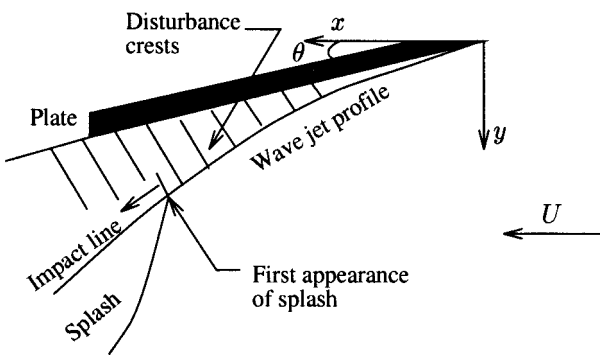

Fig. 16 Schematic of top view of bow wave indicating crests of surface disturbances

High speed videos were used to estimate the wavelength and velocity of the disturbances. Figure 18 reproduces one frame from a high speed video of the large flume experiments. From this frame and others, the wavelength was found to range from 7 cm to 16 cm at the wave profile baseline. By tracing the progress of these surface disturbances from frame to frame, it was determined that their average velocity was 2.4 m/s, approximately the velocity in the direction of the deflecting plate, namely $2.6\cos(25 \text{ deg})$. Dividing the average velocity by the average wavelength yielded a characteristic frequency for these disturbances of 22 Hz.

The same high speed videos also were used to produce water surface time histories at two locations along the wave crest, and an example is shown in Fig. 19. Although the resolution of these time histories is poor, both a lower frequency component and a higher frequency component can be observed. The lower frequency is approximately 1 Hz, and it is likely that it originates

(a) Leading portion of wave.

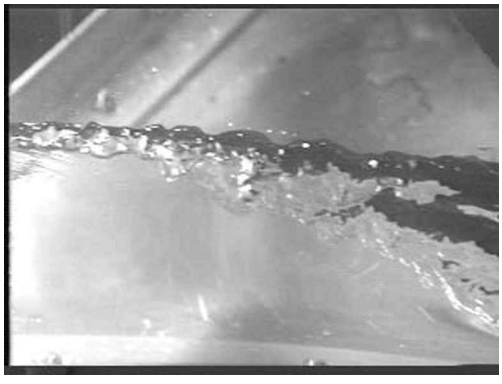

(a) Middle portion of wave.

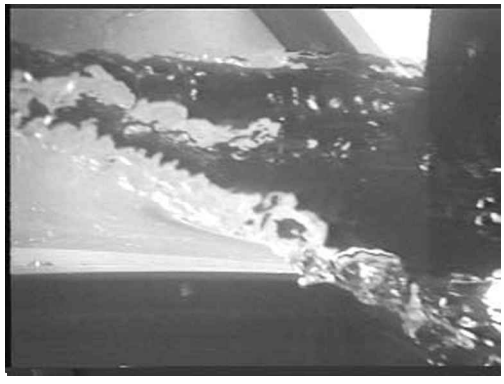

(a) Trailing portion of wave.

Fig. 17 A frame from video of surface disturbances observed in towing tank experiments. The wedge is moving to left and $\theta = 26$ deg, $\phi = 0$ deg, $U = 2.49$ m/s, $d = 7.54$ cm, and $\mathbf{F}_1 = 2.90$

from the flow conditions in the 40 m flume. The higher frequency component, estimated by counting local maxima within fixed time intervals, was between 15 Hz and 20 Hz. This is close to the surface disturbance frequency measured from video images of the traveling wave disturbances mentioned earlier.

Three wave gages flush-mounted on the surface of the deflecting plate also were used to produce time histories of the free surface height at the plate surface. In addition, a wave gage consisting of two stretched wires was located in the upstream

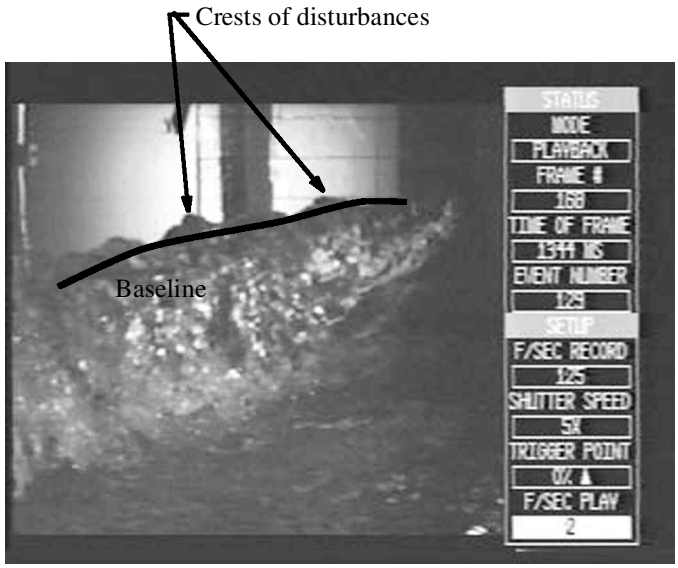

Fig. 18 A frame from high speed video of surface disturbances at trailing edge of deflecting plate. Flow is from right to left and $\mathbf{F} = 3.18$, $U = 2.64$ m/s, and $d = 7.1$ cm

reservoir to define the water surface time history there. The wave gage voltage signals were sampled at a rate of 100 Hz for 164 seconds, and post-processed using a fourth-order Butterworth filter with a cutoff frequency of 50 Hz. Examples of the filtered voltage signals are shown in Fig. 20.

Autocorrelations of the signals demonstrated that they each contained a 1 Hz component, a perturbation which was endemic throughout the flume (Waniewski 1999). Cross-correlations between wave gage records also were computed, and an example is presented in Fig. 21 for the cross-correlation between gages 1 and 3. The dominant peak occurs at 0.186 sec which, given

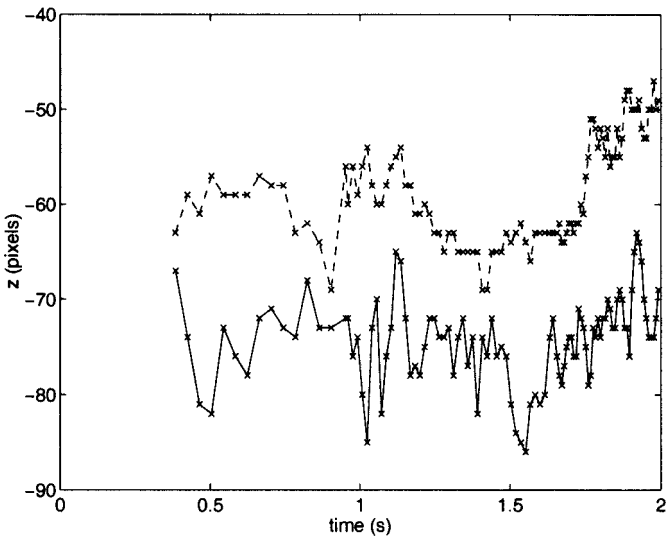

Fig. 19 Water surface time histories for two locations along surface of deflecting plate; (- -) for $r = 53.2$ cm and (—) for $r = 75.0$ cm. Flow conditions were $U = 2.64$ m/s, $d = 7.03$ cm, $\mathbf{F}_1 = 3.18$, and $\theta = 25$ deg

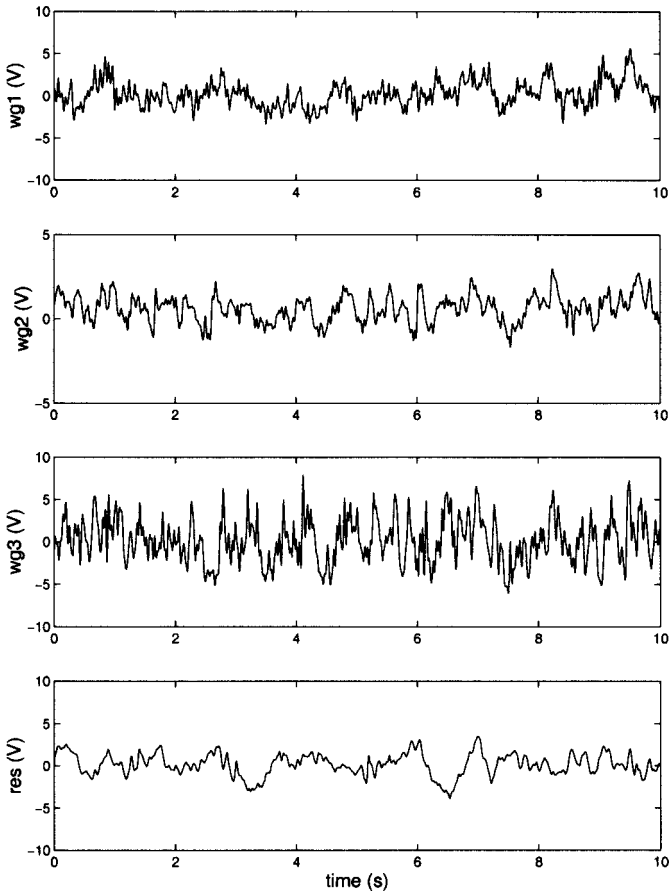

Fig. 20 Typical wave gage signals from three wave gages flush mounted on deflecting plate. Wave gage 1 (wg1) is 2.5 cm downstream of leading edge, wave gage 2 (wg2) is 20 cm downstream of leading edge, and wave gage 3 (wg3) is 40 cm downstream of leading edge. Reservoir wave gage (res) is located in upstream reservoir of 40 m flume. For these tests: $\theta \approx 26$ deg, $\phi = 0$ deg, $U = 2.69$ m/s, $d = 7.18$ cm, and $\mathbf{F}_1 = 3.21$

the distance of 37.5 cm between these gages, corresponds to a surface disturbance traveling at about 2.0 m/s. Since the liquid sheet is approximately 6 cm to 16 cm above the undisturbed free surface height, the velocity of the liquid along the contact line should be about 10% to 25% less than the incident flume, or 2.0 m/s to 2.5 m/s. Thus, it appears that the disturbances move along the face of the plunging wave at the flow velocity. The other cross-correlations yielded similar results (Waniewski 1999).

To further examine the frequencies of the surface disturbances, fast Fourier transforms (FFTs) of the signals were calculated. Figure 22 presents typical averaged, smoothed FFTs for the four wave gages. It clearly shows a difference in the frequency content of the signals from the reservoir and the three wave gages on the plate. The spectra from the plate wave gages show greater energy and a more uniform distribution of energy between 10 Hz and 25 Hz than the spectrum from the reservoir gage. It is believed that this frequency range corresponds to the surface disturbances. Using this frequency range and the velocity calculated from the cross-correlations, a range of characteristic lengths for the disturbances was found to be 8 cm to 20 cm.

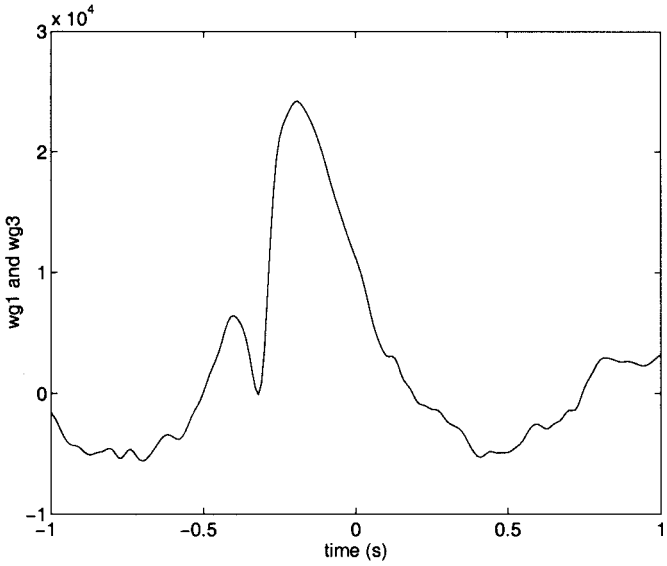

Fig. 21 A typical cross correlation for signals from wave gages 1 and 3 on deflecting plate (wg1 and wg3) shown in Fig. 20

Table 3 summarizes the measurements of frequency, velocity, and characteristic length of the surface disturbances using the two techniques on the bow wave and using the wave gages on the plate. All techniques yielded similar results, a 1 Hz frequency induced by flow conditions and higher frequencies from the surface disturbances.

10. Discussion of surface disturbances

The surface disturbances were observed in both the flume and the towing tank experiments; therefore, we would expect to see them on bow waves caused by moving ships. Similar surface

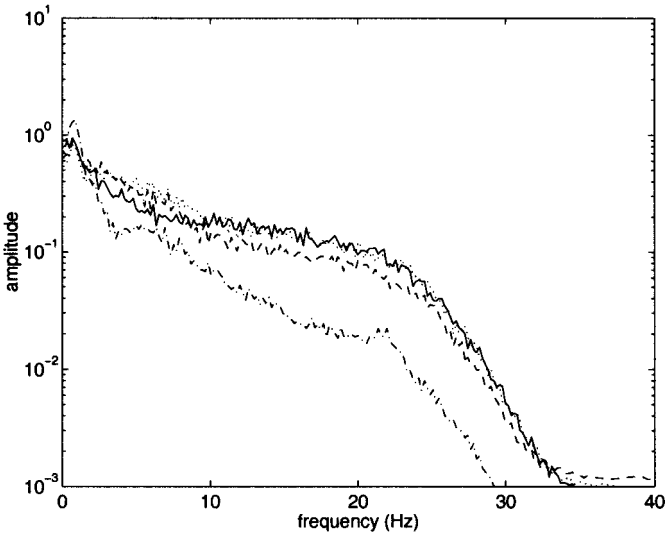

Fig. 22 Averaged fast Fourier transform over five data runs for flow conditions listed in Fig. 20. Each line represents data from a different gage: (- -) for wg1, (–) for wg2, (···) for wg3, and (-·) for res

Table 3 Summary of results from different measurement techniques used to study surface disturbances observed on bow wave

Measurement technique	From high speed video camera?	Measurement location	Frequency (Hz)	Velocity (m/s)	Characteristic length (cm)
Tracings of disturbances	Yes	Bow wave	22	2.42	7–16
Water surface time histories	Yes	Bow wave	1, 15–20	N/A	N/A
Electronic wave gages	No	Deflecting plate	1, 10–25	2.0	8–20

disturbances also can be observed in the photographs of plunging jets during wave breaking shown by Tulin & Waseda (1999).

We postulate that the surface disturbances are gravity waves which propagate along the bow wave oriented as shown in Fig. 16. Longuet-Higgins (1995) describes a similar situation in his analytical discussion of the disintegration of the jet in a plunging breaker. He begins by assuming a perturbation in the form of short surface waves, or gravity waves, which propagate across the jet surface perpendicular to the plunging jet direction. As the wave breaks and the jet stretches, the fluid begins a state of free-fall. This causes the perturbation waves to transition from gravity to capillary waves, and this transition increases their amplitude substantially. In the case of perturbations symmetric on both sides of the jet, Longuet-Higgins found that they will grow again relative to the jet thickness as the jet is stretched even further and can pinch the sheet into "cylindrical drops" or "jets."

This hypothesis and discussion are a plausible explanation for the breakup of the present plunging wave jet by the surface disturbances. In the present experiments, strings of droplets similar to Longuet-Higgins' "cylindrical drops" were seen to form on the edge of the plunging wave jet as illustrated in the photographs from the large flume in Fig. 5(a) and from the towing tank in Fig. 23. It seems that the size and spacing of the strings of droplets are controlled by the size of the surface disturbances.

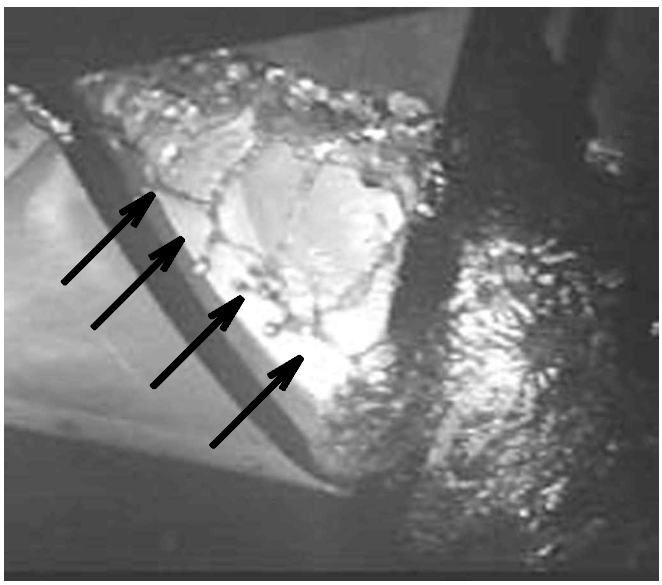

Fig. 23 A frame from video of breakup of plunging wave jet into strings of droplets (indicated by arrows) in towing tank experiments. The wedge is moving to left and $\theta = 26$ deg, $\phi = 0$ deg, $U = 2.99$ m/s, $d = 25.14$ cm, and $\mathbf{F}_2 = 1.91$

It is also possible that the disturbances originate from an instability in the flow as it passes over the deflecting plate. Observations of instabilities developing in liquid sheets on solid surfaces are not unique. For example, Shroff & Liepmann (1997) reported two-dimensional instabilities on a water sheet which developed as the sheet moved over a curved solid surface and persisted even after it left the surface.

11. Conclusions

Experimental measurements of the geometry of breaking bow waves were obtained from the waves generated by a deflecting plate in a supercritical flow in flumes at two scales and also from the bow wave created by a towed wedge with a half angle equal to the deflecting angle of the stationary plate in the flume. The contact line was measured using free-surface probes in the small and large flume experiments, and the bow wave profile was measured in the towing tank and large flume experiments using videos. These experimental results and those of Ogilvie (1972) were compared and demonstrate that the flume experiments with a depth equal to the draft produce bow waves similar to towing tank experiments with finite draft and essentially infinite depth for the same Froude number, **F**. The bow wave flow is highly nonlinear, and there appears, at present, to be no satisfactory analytical solution to this flow.

The experimental data describing the bow wave shape scales with $U^2 d^{1/2}$ in the vertical direction and with $U^2 d^{-3/2}$ in the direction along the plate. This does not agree with any theoretical scaling reported in the literature. Scaling with geometric parameters such as bow half angle and dihedral angle were investigated using contact line data, and it was found that the wave is only weakly dependent on dihedral angle and depends on the bow half-angle according to a relationship which is close to linear.

Surface disturbances with crests oriented in the cross-stream direction were observed on the plunging face of the bow wave in both the flume and the towing tank experiments. In the large flume experiment, the disturbances appear to be related to water surface oscillations on the deflecting plate. The disturbances had wavelengths which ranged from 7 cm to 16 cm. They were convected downstream with the flow velocity in the direction of the deflecting plate, and had a frequency of about 22 Hz as determined using three different experimental techniques. The disturbances are likely gravity waves on the surface of the bow wave. They grow in amplitude as the plunging jet stretches toward the free surface, and seem ultimately responsible for the breakup

of the jet into strings of droplets and for the periodic nature of the bubble clouds produced by the wave breaking process. The correlation between the surface disturbances and the bubble clouds is discussed in a companion paper (Waniewski et al 2001).

Acknowledgments

The authors wish to acknowledge undergraduate student Don Kwak for his assistance with the flume experiments. They also acknowledge Rod Barr, Bob Kowalyshyn, and Jim McGurrin of Hydronautics Research for their assistance with the towing tank experiments. In addition, they are grateful for the support of the Office of Naval Research under grant number N00014-94-1-1210, technical monitor Dr. Edwin Rood.

References

Baldy, S. 1993 A generation-dispersion model of ambient and transient bubbles in the close vicinity of breaking waves. *Journal of Geophysical Research*, **98**, C10, 18277–18293.

Carrica, P., Bonetto, F., Drew, D., and Lahey, R., Jr. 1998 A polydisperse approach to the two-phase flow around a ship. Third International Conference on Multiphase Flow, Lyon, France, June.

Dong, R., Katz, J., and Huang, T. 1997 On the structure of bow waves on a ship model. *Journal of Fluid Mechanics*, **346**, 77–115.

Fontaine, E. and Cointe, R. 1997 A slender body approach to nonlinear bow waves. *Phil. Trans. R. Soc. London A*, **355**, 565–574.

Fontaine, E. and Faltinsen, O. 1997 Steady flow near a wedge shaped bow. 12th International Workshop on Water Waves and Floating Bodies, Marseille, 75–79.

Fontaine, E. and Tulin, M. 1998 On the prediction of nonlinear free-surface flows past slender hulls using 2d+t theory: the evolution of an idea. Symposium NATO/AVT on Fluid Dynamics problems of vehicles operating near or in the air sea interface, Amsterdam, 26.1–26.10.

Joo, S., Schultz, W., and Messiter, A. 1990 An analysis of the initial-value wavemaker problem. *Journal of Fluid Mechanics*, **214**, 161–183.

Longuet-Higgins, M. 1995 On the disintegration of the jet in a plunging breaker. *Journal of Physical Oceanography*, **25**, 10, 2458–2462.

Miyata, H. and Inui, T. 1984 Non-linear ship waves. *Advances in Applied Mechanics*, **24**, 215–288.

Noblesse, F. 1983 A slender-ship theory of wave resistance. Journal of Ship Research, **27**, 1, 13–33.

Noblesse, F., Hendrix, D., and Kahn, L. 1991 Nonlinear local analysis of steady flow about a ship. Journal of Ship Research, **35**, 4, 288–294.

Ogilvie, F. 1972 The wave generated by a fine ship bow. 9th Symposium on Naval Hydrodynamics, 1483–1524.

Peltzer, R. 1984 White-water wake characteristics of surface vessels. NRL Memorandum Report 5335. Naval Research Laboratory, Washington, DC, June.

Shroff, S. and Liepmann, D. 1997 Spray generation over curved surfaces. ASME Fluids Engineering Division, June.

Tulin, M. and Waseda, T. 1999 Laboratory observations of wave group evolution, including breaking effects. *Journal of Fluid Mechanics*, **378**, 197–232.

Waniewski, T. 1999 Air entrainment by bow waves. Doctoral dissertation, California Institute of Technology, Pasadena, California.

Waniewski, T., Brennen, C., and Raichlen, F. 2001 Measurements of air entrainment by bow waves. *Journal of Fluids Engineering*, **123**, 57–63.